buildings

MDPI

Article

A Study of the Performance of Short-Column Aggregate Concrete in Rectangular Stainless Steel Pipes under Axial Compression

Ruiqing Zhu [1,2,*], Chuanyu Shao [1,2] and Haitao Chen [1,2]

[1] Shandong Provincial Key Laboratory of Civil Engineering Disaster Prevention and Mitigation, Shandong University of Science and Technology, Qingdao 266590, China; sdkjdscy@sina.com (C.S.); skdtjxycht@sdust.edu.cn (H.C.)
[2] College of Civil Engineering and Architecture, Shandong University of Science and Technology, Qingdao 266590, China
* Correspondence: sdnyzrq@gmail.com

Abstract: In this study, 18 short-column lightweight ceramsite concrete samples were prepared in rectangular stainless steel pipes, which were used for axial pressure performance tests that took the cross-sectional length–width ratio of the rectangular stainless steel pipe (1.0, 1.5 and 2.0), the wall thickness of the steel pipe (3 mm, 4 mm and 5 mm), and the strength grade of the filled concrete (C20 and C30) as the main parameters. Then, the failure patterns, axial load–displacement curve, axial load–strain curve, ultimate bearing capacity and the interaction between the steel pipe and concrete in the specimens were measured. The test results revealed that the short-column concrete specimens in the steel pipes exhibited typical shear failure and "waist-bulging" failure under axial compressive loads. In the elastic stage, the bearing capacity of the specimens was able to reach 65–85% of the ultimate bearing capacity, with the residual bearing capacity essentially reaching 70% of the ultimate bearing capacity. Furthermore, the ultimate bearing capacity of the specimens demonstrated an increase with the rise in the strength grade of the filled concrete, with the thickness of the stainless steel pipe and with the decrease in the length–width ratio of the steel pipe cross-section. The specimens exhibited a distinct hoop effect. As the length–width ratio decreased and the hoop coefficient increased, the ductility coefficient and the strength enhancement coefficient basically displayed an increasing tendency, while the concrete contribution ratio exhibited a decreasing trend.

Keywords: LWAC; concrete-filled stainless steel pipe; aggregate concrete; short column; damage patterns; ultimate bearing capacity of axial pressure; length–width ratio

Citation: Zhu, R.; Shao, C.; Chen, H. A Study of the Performance of Short-Column Aggregate Concrete in Rectangular Stainless Steel Pipes under Axial Compression. *Buildings* **2024**, *14*, 704. https://doi.org/10.3390/buildings14030704

Received: 29 January 2024
Revised: 1 March 2024
Accepted: 3 March 2024
Published: 6 March 2024

1. Introduction

Compared with ordinary concrete, lightweight aggregate concrete (LWAC) is characterized by being lightweight with high response strength, thermal insulation, durability, impermeability, shock absorption and noise reduction. In recent years, LWAC has been increasingly used in high-rise buildings and large-span bridge projects around the world, such as the One Shell Plaza in Houston [1], the Zhuhai International Convention and Exhibition Center [2] and the Tianjin Yongding New River Bridge [3]. LWAC boasts great application prospects. Many scholars have studied the mechanical properties of LWAC and found that the strength and elastic modulus of it are not significantly lower than those of ordinary concrete, but the ductility of the descending section of its compressive stress–strain curve is poor [4,5]. Therefore, it is necessary to apply external constraints to improve the ductility of LWAC. Pouring LWAC into steel pipes to form a steel pipe LWCA structure can effectively solve the problem of its brittleness.

Scholars across the globe have conducted experimental studies on the axial compression performance of steel pipe LWAC. Zhu Hongbing et al. [6] carried out axial compression performance tests on short-column specimens of micro-expansion LWAC in circular and

rectangular steel pipes, and the results showed that there was still a significant hoop effect, which is similar to the axial compression failure process of ordinary concrete. Zheng Hongyu et al. [7] conducted axial compression performance tests on short-column specimens of LWAC confined in a thin-walled circular steel pipe. The results showed that, compared to columns free from the constraints of the steel pipe, the axial compression bearing capacity increased by nearly 50%, and the displacement ductility coefficient exceeded 3.0. Li Xiu et al. [8] conducted axial compression performance tests on short-column specimens of micro-expansion LWAC in a circular steel pipe. The results showed that, within the experimental expansion agent dosage, the axial compression bearing capacity of the specimens gradually increased with increasing expansion agent dosage. Wang Yuhang et al. [9] conducted axial compression performance tests on short-column specimens of LWAC constrained by a circular steel pipe. The results showed that the specimens demonstrated good plasticity, and there was no significant decrease in the axial compression load–displacement curve. Guan et al. [10] conducted axial compression performance tests on short-column specimens of coal-gangue LWAC restrained by FRP. The results showed that coal-gangue LWAC demonstrated high porosity and low strength, making its failure brittle, and that external FRP pipe confinement can significantly improve its strength and ductility.

Using stainless steel instead of carbon steel to prepare LWAC specimens can improve the mechanical properties of steel-pipe concrete and greatly reduce engineering maintenance costs, which has important engineering significance [11–16]. Rectangular cross-sections offer greater bending stiffness, as do well-connected nodes and carefully planned layouts. These features have significant engineering importance [17–19]. To further promote the use of LWAC samples in stainless steel pipes, we carried out a systematic study on their axial compression performance to improve their safety and durability throughout their entire life cycle. However, most studies tend to focus on the structure of plain concrete-filled stainless steel tubes or LWAC-filled carbon steel tubes, with fewer studies on LWAC-filled stainless steel tube stub columns. In this study, we conducted axial compression performance tests on 18 short-column LWAC samples in rectangular stainless steel pipes. These tests used the length–width ratio of the cross-section, the wall thickness of the steel pipe, and the strength grade of the filled LWAC as variable parameters. We thereby investigated the mechanical properties and failure mechanism under axial loads, which can provide a reference for engineering applications and for the theoretical analysis of such samples.

2. Specimen Introduction

2.1. Test Design

In this test, we selected and used an austenitic S304 seamless stainless steel pipe as the outer steel pipe. This was filled with LWAC, and a total of 18 short-column LWAC-filled rectangular stainless steel pipes were prepared. The main parameters of each specimen are shown in Table 1: a height of 360 mm for all specimens; nominal wall thicknesses of 3 mm, 4 mm and 5 mm for steel pipes; and strength grades of C20 and C30 for the LWAC. The cross-sections of specimens are shown in Figure 1. For example, specimen No. "C6-T3-2" represents a rectangular stainless steel pipe specimen with a width of 60 mm, a nominal pipe wall thickness of 3 mm and a concrete strength grade of C20. a, b and t are the cross-sectional length, width and thickness of rectangular stainless steel pipes, respectively; a/b is the length–width ratio; ξ is the hoop coefficient, defined as $\xi = f_y A_s / f_{ck} A_c$ [20]; N_u is the tested value of the bearing capacity, *SI* is the strength index; and *DI* is the ductility coefficient.

The preparation process of the specimens is shown in Figure 2. Firstly, the cross-sections at both ends of the steel pipe were flattened in the factory to ensure that the specimen was kept perpendicular to the loading end during loading. The bottom of the steel pipe was connected to the flat plate in advance, and the joints were sealed with silicone adhesive. Furthermore, the ceramisite was pre-wet. During casting, the concrete

was cast layer by layer and fully compacted with a vibrating rod to ensure compactness. After casting was completed, the surface of the concrete needed to be slightly higher than the surface of the stainless steel pipe and covered with plastic film. The specimens were naturally cured for 28 days. Before the test, the specimens were peeled off from the flat plate and a polishing machine was used to smooth both ends of the specimens.

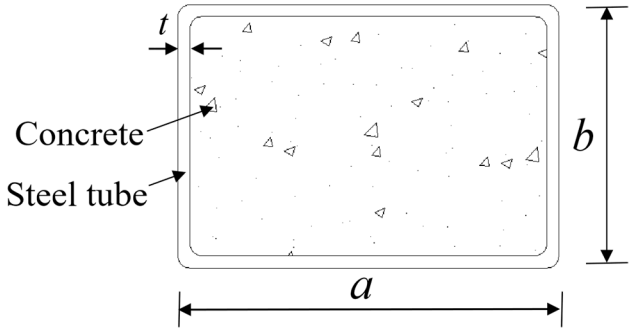

Figure 1. Cross-sections of specimens.

(**a**) Connect to flat plate and seal with silicone adhesive

(**b**) Pre-wet ceramisite

(**c**) Cast concrete and cover it with film

(**d**) Polish concrete

Figure 2. Manufacturing process of specimens.

Table 1. Parameters of specimens.

Specimen No.	*a*/mm	*b*/mm	*a*/*b*	*t*/mm	N_u/kN	ξ	*DI*	*SI*	*CCR*
C6-T3-2	120	60	2.0	2.53	660	2.58	2.53	1.04	1.82
C6-T3-3	120	60	2.0	2.55	674	2.05	1.90	0.99	1.86
C6-T4-2	120	60	2.0	4.11	903	5.06	2.62	0.92	1.23
C6-T4-3	120	60	2.0	4.13	1037	4.06	2.23	1.01	1.36
C6-T5-2	120	60	2.0	5.21	1247	6.82	2.32	1.04	1.43
C6-T5-3	120	60	2.0	5.22	1366	5.48	2.29	1.11	1.57
C8-T3-2	120	80	1.5	2.51	739	2.07	2.01	0.99	1.42

Table 1. *Cont.*

Specimen No.	*a*/mm	*b*/mm	*a*/*b*	*t*/mm	N_u/kN	ξ	*DI*	*SI*	*CCR*
C8-T3-3	120	80	1.5	2.52	848	1.67	2.07	1.05	1.63
C8-T4-2	120	80	1.5	4.41	990	4.40	2.72	0.83	1.53
C8-T4-3	120	80	1.5	4.41	1101	3.54	1.88	0.88	1.79
C8-T5-2	120	80	1.5	5.42	1522	5.68	2.51	1.07	1.18
C8-T5-3	120	80	1.5	5.42	1680	4.56	2.71	1.14	1.46
C12-T3-2	120	120	1.0	2.83	1002	1.85	1.72	0.96	1.40
C12-T3-3	120	120	1.0	2.83	1375	1.48	1.87	1.21	1.93
C12-T4-2	120	120	1.0	4.41	1714	3.40	2.45	1.12	1.52
C12-T4-3	120	120	1.0	4.43	1723	2.74	2.20	1.06	1.52
C12-T5-2	120	120	1.0	5.44	2094	4.36	2.16	1.15	1.16
C12-T5-3	120	120	1.0	5.44	2308	3.49	2.02	1.22	1.28

2.2. Material Performance

According to the provisions of *Metallic Materials—Tensile Testing—Part 1: Method of Test at Room Temperature* (a Chinese national standard numbered GB/T228.1-2021) [21], we conducted tensile tests on stainless steel pipes of three different thicknesses, and their main mechanical performance indicators are shown in Table 2. The design strength grades of LWAC are C20 and C30, and the proportioning ratio is shown in Table 3. The coarse aggregate is Grade 800 shale ceramsite with a particle size of 5 mm to 10 mm and a bulk density of 762 kg/m^3. According to the *Standard for Test Methods of Concrete Physical and Mechanical Properties* (a Chinese national standard numbered GB/T 50081-2019) [22], we conducted cubic compressive strength (f_{cu}) tests on two types of LWACs, and the measured results are shown in Table 3.

Table 2. Mechanical properties of stainless steel.

Type	*t*/mm	f_u/MPa	E_s/MPa	δ/%
Austenite 304	3	512	181,657.2	35.57
	4	579	203,637.7	25.00
	5	588	201,714.5	37.57

Notes: The results shown in the table are the average values of the three specimens of each thickness. E_s represents the elastic modulus of the stainless steel pipe, f_u is the ultimate tensile strength, δ is the elongation rate and μ_s is the Poisson's ratio.

Table 3. Proportioning ratio of LWAC.

Strength Grade	Composition/(kg·m^{-3})					Water–Binder Ratio	f_{cu}/MPa
	Cement	Aggregate	Sand	Water	Water–Reducer		
C20	390	569.6	619.9	180	3.9	0.46	28.05
C30	420	633.8	700.7	164	4.2	0.39	37.91

2.3. Test Loading Scheme and Measurement Point Arrangement

We employed the YYAW40500 microcomputer-controlled electro-hydraulic servo pressure tester for axial pressure performance testing. The loading site and loading device are shown in Figure 3. We implemented pre-loading before formal loading, the pre-loading is performed before formal loading to verify the data and eliminate the impact of gaps on the experiment, with the loading value not exceeding 10% of the estimated bearing capacity. During formal loading, the specimens were loaded using force control at a rate of 2 kN/s before yielding; after the specimens reached the yield stage, the loading was based on displacement control at a rate of 0.6 mm/min until the specimens failed and the loading was terminated. Conditions for termination of test loading: (1) Fracture occurs on the surface of the specimen; (2) The residual bearing capacity of the specimen drops

below 70% of the test ultimate load; (3) The axial deformation of the specimen exceeds the specified requirement for axial compression deformation or there is a situation where it is deemed inappropriate to continue loading. The measurement device for the test is shown in Figure 3b, with a total of 16 strain gauges arranged on the surface of the steel pipe to detect the longitudinal and transverse strains of the outer steel pipe. In addition, six displacement meters (D1–D6) were provided between the upper and lower loading plates of the tester and in the middle of the specimens to verify the vertical displacement of the loading system and the lateral displacement of the specimens.

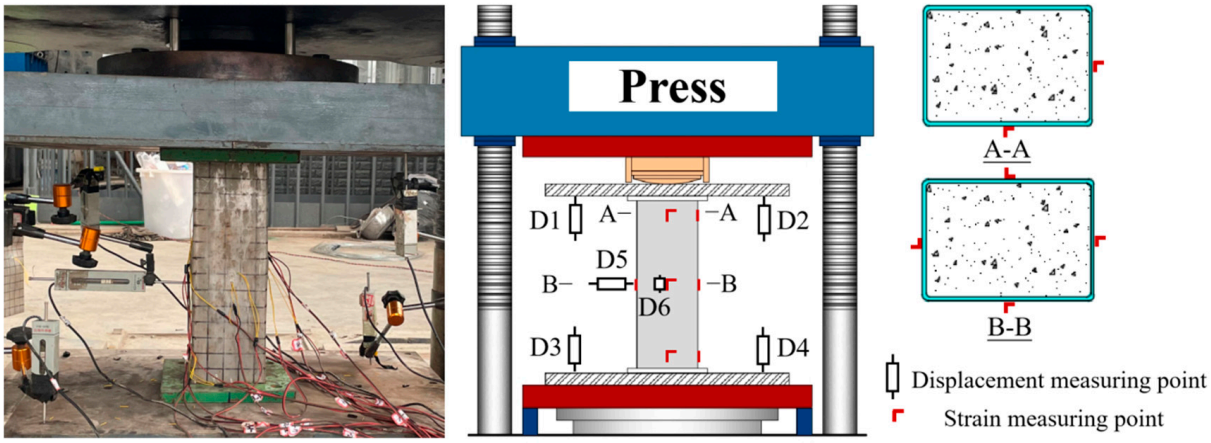

(**a**) Loading site (**b**) Loading and measurement device

Figure 3. Test loading device.

3. Test Results and Analysis

3.1. Test Phenomenon

Figure 4 shows the failure modes of each specimen, while Figure 5 shows the post-test failure of internal concrete after cutting off the outer steel pipe. It can be observed that the failure modes of the specimens are mainly divided into shear failure and "waist-bulging" failure. Taking the specimen numbered C8-T4-3 as an example, during the initial loading stage, there was no significant damage to the surface of the stainless steel pipe. When the axial load was applied to 85% of the peak load, slight bulging began to appear in the upper part of the specimen. When the load applied to the peak load continued to increase, the specimen bulged rapidly until it failed. The specimen exhibited shear failure with obvious shear cracks in the internal concrete, as shown in Figure 5b. Taking C6-T4-3 as another example, no changes were observed on the surface of the specimen during the initial loading stage. When the axial load was applied to 85% of the peak load, there was a slight bulging in the upper part of the specimen. As the loading continued to increase, the axial compression continued and the bulging gradually penetrated at the same height as the specimen, forming a significant defect until the specimen failed. The specimen exhibited a "waist-bulging" failure, and the internal concrete collapsed significantly at the defect point, as shown in Figure 5a,b. It can be thus concluded that for rectangular section specimens with $a/b > 1.0$, the degree of bulging on the shorter side of the section is significantly lower than that on the longer side, while for square section specimens with $a/b = 1$, the degree of bulging on all four sides of the section is relatively the same. This is because the rectangular section steel pipe has different degrees of constraint on the internal concrete.

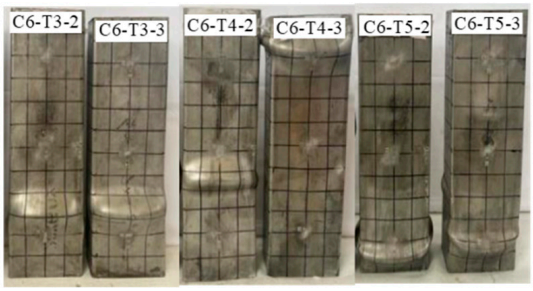

(**a**) *a*/*b* = 2.0

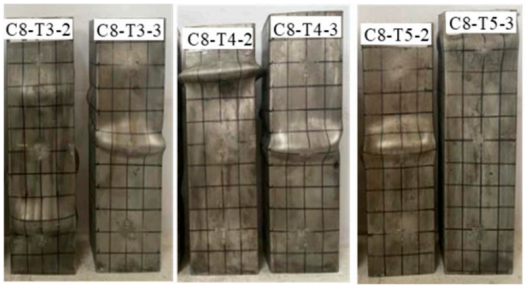

(**b**) *a*/*b* = 1.5

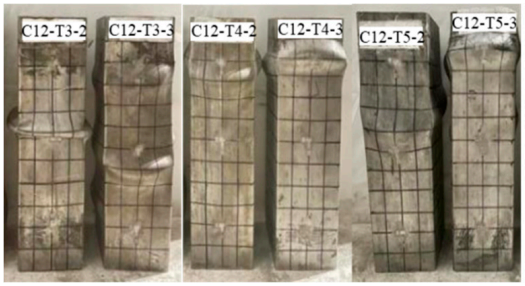

(**c**) *a*/*b* = 1.0

Figure 4. Failures of specimens.

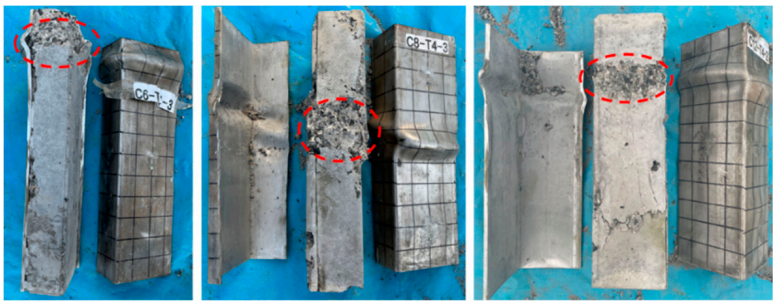

(**a**) C6-T4-3 (**b**) C8-T4-3 (**c**) C12-T4-2

Figure 5. Failures of internal concrete.

3.2. Axial Load–Strain Curve

Figure 6 shows the axial load–displacement curve of each specimen. It can be observed that the development trend of the axial load–displacement curve for each specimen is roughly similar. In the initial stage of loading, the axial load–strain curve of the stainless steel tube exhibits linear growth, indicating that both the steel pipe and the core LWAC are in an elastic working state. It is important to note that the growth rate of longitudinal strain is consistently greater than that of transverse strain at this stage and the ratio of longitudinal strain to transverse strain is close to the Poisson's ratio of stainless steel (v = 0.3). The study concludes that the stainless steel tube does not have a confinement effect on the concrete during the elastic stage. When the axial load was applied to 65–85% of the peak load, the axial stiffness gradually decreased and the slope of the curve began to decrease. The most likely cause of this is the formation and development of micro-cracks in the concrete. At this time, the specimen is in the elastic–plastic stage, the Poisson's ratio (ν) increased rapidly within the range of 0.3–0.7 until the axial load approached the ultimate load capacity (N_u), indicating the confinement effect of the stainless steel pipes on the concrete; the restraining effect of stainless steel pipes on the specimen can delay the internal concrete failure, thereby improving its compressive strength and further increasing the bearing capacity of the specimen until it reached its ultimate bearing capacity. When the loading was continued, the external stainless steel pipe buckled and internal concrete cracks developed rapidly.

Due to the stress redistribution between the steel pipe and concrete, the load shown on the descending section of the curve steadily decreased and the residual bearing capacity of each specimen reached 70% of the ultimate bearing capacity. The descending section of the curves of specimens C8-T4-2 and C8-T4-3 shows a slight upward trend, mainly due to the readjustment of the steel pipe after compression buckling, which enhances the constraint effect on the internal concrete.

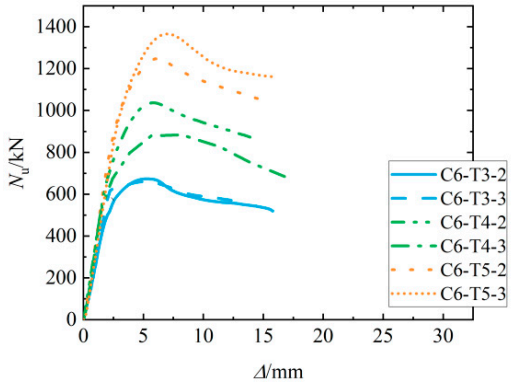

(**a**) a/b = 2.0

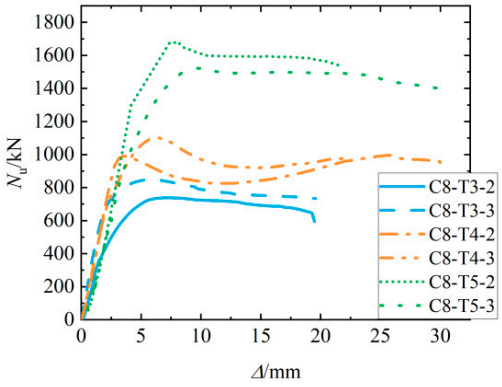

(**b**) a/b = 1.5

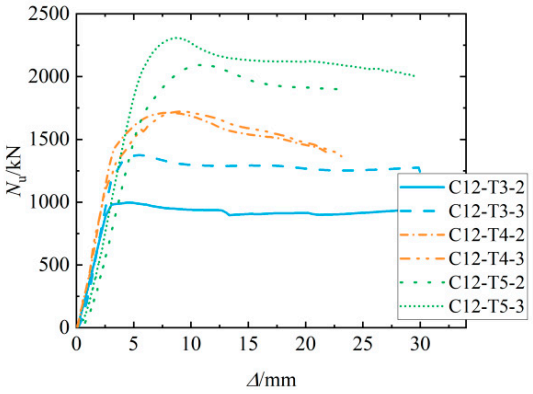

(**c**) a/b = 1.0

Figure 6. Load–axial displacement curve.

3.3. Axial Load–Strain Curve

Figure 7 shows the axial load–strain curve of each specimen, with the longitudinal compressive strain curve on the right and the transverse tensile strain curve on the left. It can be observed that the development trend of axial load–strain curve for each specimen is roughly similar. In the initial stage of loading, the curve shows a linear growth trend, and both the stainless steel pipe and the internal concrete bore stress independently. At this time, the specimens were in the elastic stage, and the longitudinal strain growth rate of the steel pipe was greater than the transverse strain. When the loading was continued and the specimens reached the elastic–plastic stage, the slope of the curve began to decrease. At this time, due to the interaction between the external stainless steel pipe and the internal concrete, the growth rate of the transverse strain of the steel pipe generally increased. However, due to the uneven constraint effect of the rectangular section steel pipe on the internal concrete, the transverse strain of some strain gauges in the steel pipe decreased. When the ultimate bearing capacity of the specimens was reached, internal concrete cracks developed rapidly, the bonding between the internal concrete and external stainless steel pipe failed, the buckling deformation of the external stainless steel pipe continued to grow and the rate of the lateral strain development of the steel pipe further increased. In addition,

the strain gauges of specimen C6-T4-2 exhibited poor adhesion during the later stage of loading, resulting in a slight degree of decrease in the curve.

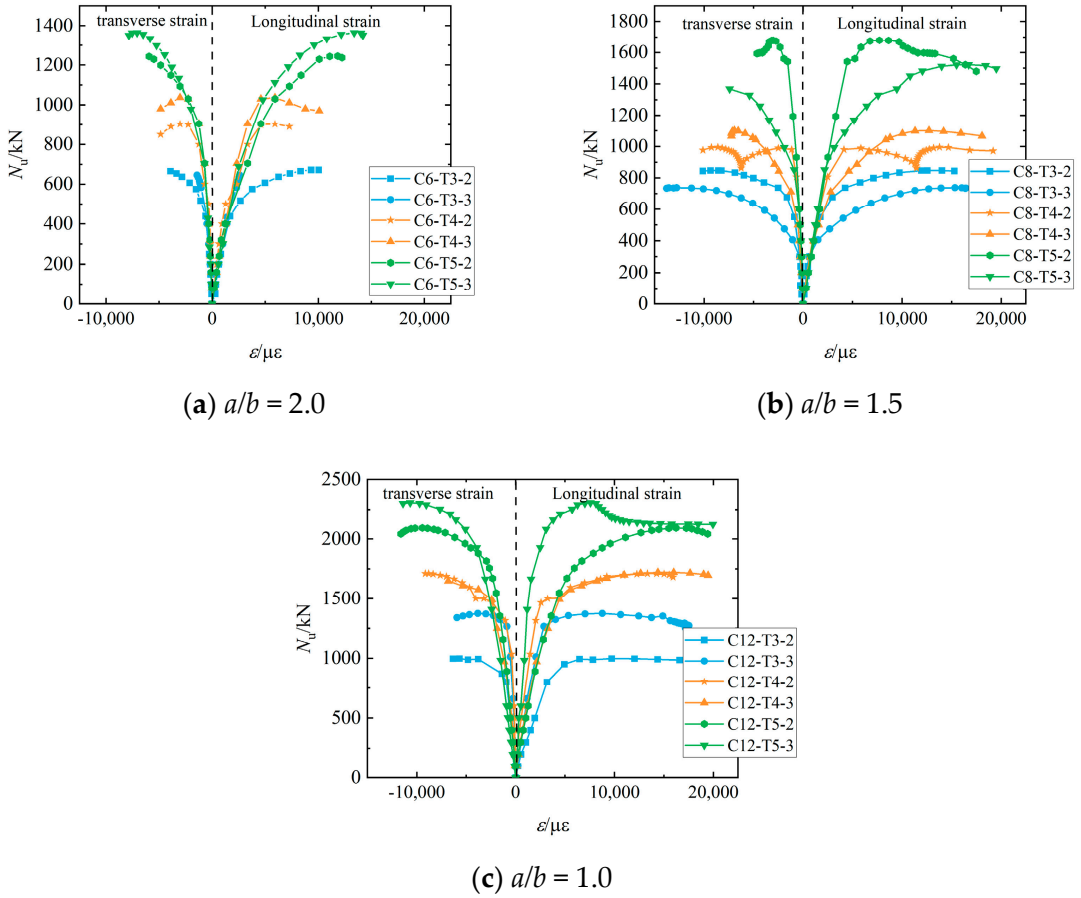

(**a**) a/b = 2.0 (**b**) a/b = 1.5

(**c**) a/b = 1.0

Figure 7. Load−strain curves of specimen.

3.4. Ultimate Bearing Capacity

Figure 8 shows the test results of the ultimate bearing capacity of each specimen. It can be observed that the ultimate bearing capacity of each specimen increases with increasing strength grade of the filled LWAC. When the strength grade of it was increased from C20 to C30, the average increase in the ultimate bearing capacity of the specimen with different length–width ratios and thicknesses of stainless steel pipes was 12.3%. When the strength grade was increased from C20 to C30, the increase in the ultimate bearing capacity of the specimen with a 3 mm thick stainless steel pipe and a length–width ratio of 1.0 was as high as 37%.

As shown in Figure 8, the ultimate bearing capacity of each specimen increases with increasing stainless steel pipe thickness. When the thickness of the stainless steel pipe increased from 3 mm to 4 mm, the average increase in the ultimate bearing capacity of specimens with different strength grades of filled concrete and different length–width ratios could reach 42%. When the thickness increased from 4 mm to 5 mm, the average increase could reach 39%. This is mainly because the increase in stainless steel pipe thickness increased the confinement coefficient of the specimens (as shown in Table 1). The external steel pipe demonstrated a certain degree of improvement in the restraining effect on the filled concrete, helping resolve the brittleness of the filled concrete and thus increasing the ultimate bearing capacity of the specimens.

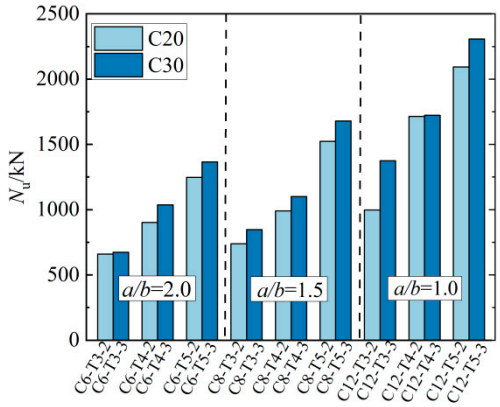

Figure 8. Comparison of ultimate bearing capacity specimens.

As shown in Figure 8, the ultimate bearing capacity of each specimen increases with decreasing length–width ratio, mainly due to the increase in the areas of stainless steel pipes and concrete in the cross-section of the specimen. When the length–width ratio of the specimen section was reduced from 2.0 to 1.5, the cross-sectional area of the specimen increased by 33.3%. The average increase in the ultimate bearing capacity of specimens with different strength grades of filled concrete and different thicknesses of stainless steel pipes was 16.4%. When the length–width ratio was reduced from 1.5 to 1.0, the cross-sectional area increased by 50.4%. The average increase was 50.0%.

4. Analysis of Interaction between Steel Pipes and Concrete

For LWAC columns in rectangular stainless steel pipes, filling the inside with concrete can increase the stability of the external stainless steel pipe and prevent local instability. Moreover, the stainless steel pipe can effectively constrain the filled concrete, helping increase its strength under triaxial compression.

4.1. Ductility Coefficient

We used *DI*, the ductility coefficient, to quantitatively evaluate the deformation capacity of the specimens [23]. As expressed in Equation (1), the higher the value of *DI*, the better the deformation capacity of the specimen. Table 1 lists the ductility coefficient of each specimen.

$$DI = \frac{\Delta_{85\%}}{\Delta_u} \quad (1)$$

In Equation (1), $\Delta_{85\%}$ represents the displacement that corresponds to a load drop of 85% of the peak load. Alternatively, $\Delta_{85\%}$ can be used as the displacement corresponding to the first valley on the axial load displacement curve, i.e., the valley displacement for specimens where the load has not dropped to 85% of the peak load [24]. Δu represents the displacement corresponding to the peak load.

Figure 9 shows the relationship between the ductility coefficient and the hoop coefficient of each specimen. It can be observed that the ductility coefficient of each specimen ranges from 1.72 to 2.72. As the length–width ratio decreased, the ductility coefficients of each specimen showed an increasing trend. As the hoop coefficient increased, the ductility coefficients of each specimen showed an increasing trend, indicating that the closer the cross-section of the specimen is to a square, the greater the hoop coefficient and the better the restraining effect of the external stainless steel pipe on the filled concrete. The ductility coefficient of the specimen with a hoop coefficient of between 1 and 3 increased by an average of 13.7% compared to the specimen with a hoop coefficient between 3 and 5. However, when the hoop coefficient was greater than 5, the ductility coefficient did not continue to increase. This is because the filled LWAC, with lower strength, failed to delay the local

buckling deformation of the external stainless steel pipe, and the combined advantages of the concrete and steel pipe were not fully leveraged.

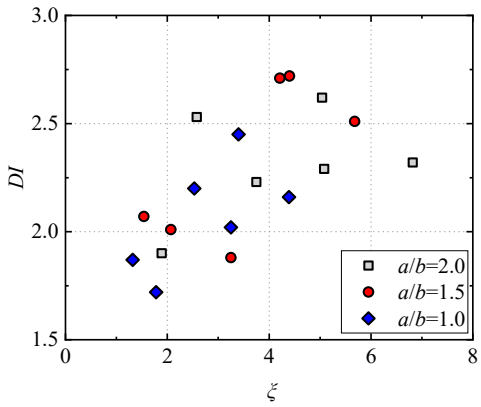

Figure 9. Relationship between the ductility coefficient and the hoop coefficient.

4.2. Strength Enhancement Coefficient

The strength enhancement coefficient SI is used to quantitatively evaluate the influence of the interaction between a steel pipe and concrete on the ultimate bearing capacity of the specimen [25], as expressed in Equation (2). The larger the value of the SI, the more significant the restraining effect of the steel pipe on concrete is, and the stronger the interaction effect between the two, the more significant the enhancement in the ultimate bearing capacity. Table 1 lists the strength enhancements of each specimen.

$$SI = \frac{N_u}{f_y A_s + f_{ck} A_c} \tag{2}$$

In Equation (2), N_u is the ultimate bearing capacity of each specimen; A_s and A_c are the area of the stainless steel pipe and concrete, respectively; and f_{ck} is the standard value of the axial compressive strength of concrete.

Figure 10 shows the relationship between the strength enhancement coefficient and the hoop coefficient of each specimen. It can be observed that the strength enhancement coefficient of each specimen ranges from 0.83 to 1.22. As the length–width ratio decreased, the strength enhancement coefficient of each specimen basically showed an increasing trend, indicating that when the cross-section is closer to a square, the collaboration between the external stainless steel pipe and the filled concrete is better. As the hoop coefficient increased, the trend of the strength enhancement coefficient for each specimen was not clear. This was also due to the low strength and internal defects of the filled LWAC. The external stainless steel pipe failed to provide effective constraints on the concrete, and the combined advantages of concrete and steel pipes were not fully leveraged.

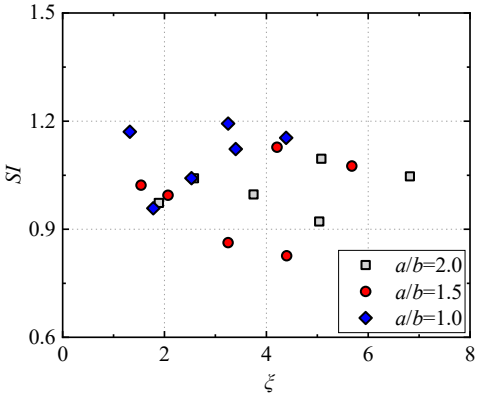

Figure 10. Relationship between strength enhancement coefficient and hoop coefficient.

4.3. Concrete Contribution Ratio

We used the concrete contribution rate (CCR) to quantitatively evaluate the improvement in the ultimate bearing capacity of the concrete-filled steel pipe specimens. CCR can be defined as the ratio of the ultimate bearing capacity of the concrete-filled steel pipe to that of the corresponding hollow steel pipe, as expressed in Equation (3). In order to obtain the ultimate bearing capacity of the corresponding hollow steel pipes, nine hollow stainless steel pipes, made of the same material and of the same size as the specimens in the same batch, underwent axial compression performance testing. The obtained bearing capacities of the hollow steel pipes is shown in Table 4. Table 1 lists the concrete contribution ratios of each specimen.

$$CCR = \frac{N_u}{N_{hollow}} \tag{3}$$

In Equation (3), N_{hollow} is the ultimate bearing capacity of each hollow steel pipe.

Table 4. Ultimate bearing capacity of hollow steel pipes.

a/*b*		2.0			1.5			1.0	
t/mm	2.53	4.05	5.11	2.49	4.39	5.43	2.82	4.42	5.43
N_u/kN	363	807	870	520	810	1237	712	1130	1800

Figure 11 shows the relationship between the concrete contribution ratio and the hoop coefficient of each specimen. It can be observed that the concrete contribution ratio of each specimen is between 1.16 and 1.93. According to Table 1, as the strength grade of the filled concrete increased, the concrete contribution ratio showed an increasing trend. As the length–width ratio increased, the concrete contribution ratio basically showed an increasing trend, indicating that the greater the length–width ratio, the greater the contribution made by the filled concrete to the specimen's strength. As the hoop coefficient increased, the concrete contribution ratio basically showed a decreasing trend, indicating that the stronger the constraining effect provided by the external stainless steel pipe, the lesser the contribution of the filled concrete to the specimen's strength.

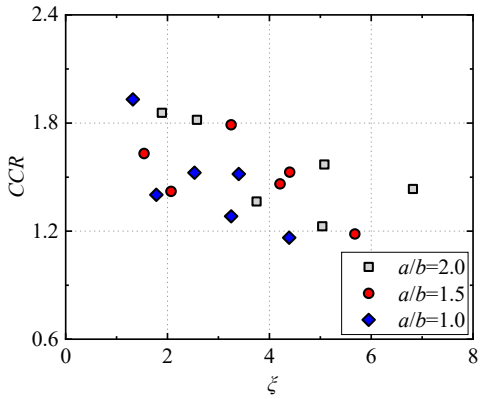

Figure 11. Concrete contribution rate versus confinement factor relationship.

5. Conclusions

(1) The axial compression failure process and failure mode of LWAC in stainless steel pipes are similar to those of concrete in ordinary steel pipes, and the failure modes mainly include shear failure and "waist-bulging" failure. The degree of bulging on the short side of the rectangular section specimen was significantly weaker than that on the long side and was unlike the failure on the four sides of the square section specimen. This is because the rectangular section steel pipe has different degrees of constraints on the internal concrete.

(2) The axial load–displacement curve of the LWAC specimens in stainless steel pipes can be mainly divided into three stages: elastic stage, elastic–plastic stage and descending stage. The bearing capacity of specimens in the elastic stage can reach 65–85% of the ultimate bearing capacity, and the residual bearing capacity can essentially reach 70% of the ultimate bearing capacity. The ultimate bearing capacity of the specimens increased with increasing strength grade of the filled concrete, with increasing thickness of the stainless steel pipe and with decreasing length–width ratio.

(3) The LWAC specimens in rectangular stainless steel pipes exhibited a significant interaction between the steel pipe and concrete. With a decrease in the length–width ratio and an increase in the hoop coefficient, the ductility coefficient and strength enhancement coefficient of each specimen showed an increasing trend, but the concrete contribution ratio showed a decreasing trend. This phenomenon indicates that, when the external stainless steel pipe has a stronger collaboration with the filled concrete, the concrete's contribution to the load-bearing capacity of the specimens is lessened.

Author Contributions: Conceptualization, R.Z. and H.C.; methodology, R.Z.; validation, R.Z. and C.S.; formal analysis, R.Z. and C.S.; investigation, C.S. and C.S.; resources, H.C.; data curation, H.C. and R.Z.; writing—original draft preparation, R.Z. and C.S.; writing—review and editing, R.Z., C.S. and H.C.; visualization, R.Z. and C.S.; supervision, H.C. and R.Z.; project administration, H.C. All authors have read and agreed to the published version of the manuscript.

Funding: This research received no external funding.

Data Availability Statement: The data presented in this study are available on request from the corresponding author. The data are not publicly available due to privacy.

Acknowledgments: The authors would like to thank the staff of Shandong Provincial Key Laboratory of Civil Engineering Disaster Prevention and Mitigation, Shandong University of Science and Technology, for their advice in the fulfillment of the current study.

Conflicts of Interest: All authors declare that they have no conflicts of interest.

References

1. Huang, C. Research on Imposed Load Test of Full-Scale Assembied Precast Shale-Ceramsite Concrete Composite Slabs. Master's Thesis, Wuhan University of Technology, Wuhan, China, 2017.
2. Peng, X.; Zhou, Y.; Jia, R.; Wang, W. Preparation of non-sintered lightweight aggregates from dredged sediments and modification of their properties. *J. Constr. Build. Mater.* **2017**, *132*, 9–20. [CrossRef]
3. Chao, C.; Yang, Y. The Properties and Benefit Analysis about Using High-Strength Light Aggregate Concrete on Bridge. *J. Concrete* **2000**, *1*, 27–29.
4. Guo, Z.; Zhang, X.; Zhang, D.; Wang, R. Experimental Investigation of the Complete Stress-Strain Curve of Concrete. *J. Build. Struct.* **1982**, *1*, 1–12.
5. Li, P.; Liu, X. Fundamental Mechanical Properties of Concretewith High Strength Expanded Shale. *J. Build. Mater.* **2004**, *1*, 113–116.
6. Zhu, H.; Zhao, B.; Li, X.; Yuan, Q.; Hu, T. Ultimate bearing capacity of micro-expansive ceramsite concrete filled rectangular steel tubular short column under axial compression. *J. Wuhan Univ. Sci. Technol.* **2019**, *42*, 68–74.
7. Zheng, H.; Zheng, J.; Ke, X.; Zhu, Z.; Meng, M.; Zheng, Y. Research on the axial compression performance of ceramic aggregate concrete short columns confined by thin-walled circular steel pipes. *J. Guangxi Univ.* **2022**, *47*, 74–82.
8. Li, X.; Zhu, H.; Han, S. Ultimate Bearing Capacity Calculation Formula of Micro-expansive Ceramsite Concrete Steel Tubular Short Column under Axial Compression. *China Concr. Cem. Prod.* **2021**, *5*, 76–79.
9. Wang, Y.; Zhao, Y.; Zhou, X.; Li, Q. Experimental Research and Bearing Capacity Calculation of Ceramsite Concrete Filled Circular Steel Tube Short Column under Uniaxial Compression. *Ind. Constr.* **2022**, *52*, 1–7.
10. Guan, H.; Xia, Y.; Zhang, S.; Wu, J.; Wang, J.; Wang, B. A theoretical axial stress–strain model for gangue ceramsite concrete confined with FRP tube. *Constr. Build. Mater.* **2022**, *350*, 128864. [CrossRef]
11. Chen, X.; Liao, F.; Lin, Z.; Ren, M. study on design approach of the circular concrete filled stainless steel tube under axial compression. *Ind. Constr.* **2020**, *50*, 137–144+152.
12. Qiao, Q.; Yang, Z.; Cao, W. Axial compressive behavior of stainless steel tube confined concrete column piers. *Mar. Struct.* **2021**, *78*, 103021.
13. Uy, B.; Tao, Z.; Han, L.H. Behaviour of short and slender concrete-filled stainless steel tubular columns. *J. Constr. Steel Res.* **2011**, *67*, 360–378. [CrossRef]

14. Tang, H.; Wang, H.; Liu, Y.; Bian, Y.; Gao, Z. Axial compressive property of square and rectangular UHPC-filled duplex stainless steel tube stub columns. *Compos. Struct.* **2023**, *323*, 117492. [CrossRef]
15. Azad, S.K.; Li, D.; Uy, B. Compact and slender box concrete-filled stainless steel tubes under compression, bending, and combined loading. *J. Constr. Steel Res.* **2021**, *184*, 106813. [CrossRef]
16. Chen, Y.; Feng, R.; Wang, L. Flexural behaviour of concrete-filled stainless steel SHS and RHS tubes. *Eng. Struct.* **2017**, *134*, 159–171. [CrossRef]
17. Mouli, M.; Khelafi, H. Strength of short composite rectangular hollow section columns filled with lightweight aggregate concrete. *Eng. Struct.* **2007**, *29*, 1791–1797. [CrossRef]
18. Schneider, S.P. Axially loaded concrete filled steel tubes. *J. Struct. Eng.* **1998**, *124*, 1125–1138. [CrossRef]
19. Ibañez, C.; Hernández-Figueirido, D.; Piquer, A. Shape effect on axially loaded high strength CFST stub columns. *J. Constr. Steel Res.* **2018**, *147*, 247–256. [CrossRef]
20. Han, L. *Steel Pipe Concrete structure: Theory and Practices*, 3rd ed.; Science Press: Beijing, Chian, 2016. (In Chinese)
21. *GB/T 228.1-2021*; Metallic Materials—Tensile Testing—Part 1: Method of Test at Room Temperature. Standards Press of China: Beijing, China, 2021.
22. *GB/T 50081-2019*; Standard for Test Methods of Concrete Physical and Mechanical Properties. China Architecture & Building Press: Beijing, China, 2019.
23. Qu, X.; Chen, Z.H.; Sun, G.J. Axial behaviour of rectangular concrete-filled cold-formed steel tubular columns with different loading methods. *Steel Compos. Struct. Int. J.* **2015**, *18*, 71–90. [CrossRef]
24. Zhang, X.; Zhou, G.; Fan, Y. Axial compressive property of circular steel tubular stub column filled with basalt fiber reinforced recycled concrete. *Acta Mater. Compos. Sin.* **2023**, *40*, 369–382.
25. Han, L.; Tao, Z. Study on behavior of concrete filled square steel tubes under axial load. *China Civ. Eng. J.* **2001**, *2*, 17–25.